Bioconjugate Chemistry

Article

pubs.acs.org/bc

Amphiphilic Macromolecule Self-Assembled Monolayers Suppress Smooth Muscle Cell Proliferation

Jennifer W. Chan,[†] Yingyue Zhang,[‡] and Kathryn E. Uhrich*[,†,‡]

[†]Department of Biomedical Engineering, Rutgers University, 599 Taylor Road, Piscataway, New Jersey 08854, United States

[‡]Department of Chemistry and Chemical Biology, Rutgers University, 610 Taylor Road, Piscataway, New Jersey 08854, United States

Supporting Information

ABSTRACT: A significant limitation of cardiovascular stents is restenosis, where excessive smooth muscle cell (SMC) proliferation following stent implantation causes blood vessel reocclusion. While drug-eluting stents minimize SMC proliferation through releasing cytotoxic or immunosuppressive drugs from polymer carriers, significant issues remain with delayed healing, inflammation, and hypersensitivity reactions associated with drug and polymer coatings. Amphiphilic macromolecules (AMs) comprising a sugar-based hydrophobic domain and a hydrophilic poly(ethylene glycol) tail are noncytotoxic and recently demonstrated a concentration-dependent ability to suppress SMC proliferation. In this study, we designed a series of AMs and studied their coating properties (chemical composition, thickness, grafting density, and coating uniformity) to determine the effect of headgroup chemistry on bioactive AM grafting and release properties from stainless steel substrates. One carboxyl-terminated AM (**1cM**) and two phosphonate- (**Me-1pM** and **Pr-1pM**) terminated AMs, with varying linker lengths preceding the hydrophobic domain, were grafted to stainless steel substrates using the tethering by aggregation and growth (T-BAG) approach. The AMs formed headgroup-dependent, yet uniform, biocompatible adlayers. **Pr-1pM** and **1cM** demonstrated higher grafting density and an extended release from the substrate over 21 days compared to **Me-1pM**, which exhibited lower grafting density and complete release within 7 days. Coinciding with their release profiles, **Me-1pM** and **1cM** coatings initially suppressed SMC proliferation in vitro, but their efficacy decreased within 7 and 14 days, respectively, while **Pr-1pM** coatings suppressed SMC proliferation over 21 days. Thus, AMs with phosphonate headgroups and propyl linkers are capable of sustained release from the substrate and have the ability to suppress SMC proliferation during the restenosis that occurs in the 3−4 weeks after stent implantation, demonstrating the potential for AM coatings to provide sustained delivery via desorption from coated coronary stents and other metal-based implants.

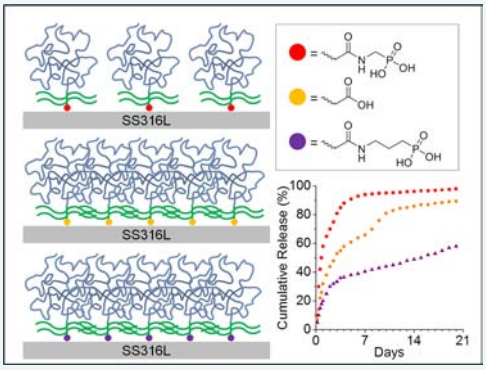

INTRODUCTION

Surface modification techniques have gained significant interest as methods to functionalize a wide range of biomaterials. Although many implants are made of medical grade metal alloys such as stainless steel, nitinol, or cobalt chrome, these materials are not biocompatible, leading to inflammatory and foreign body reactions.[1] Implant surfaces can be modified with self-assembled monolayers (SAMs), polymer brushes, or other techniques to promote implant biocompatibility integration, resistance to protein or bacterial adsorption, or mimic biological functions.[2,3] As examples, antiproliferative drugs,[4,5] bioligands,[6−9] antibiotics,[10,11] and other actives have been directly coated or incorporated into implant coatings to provide localized therapeutic delivery and minimize systemic toxicity associated with these actives.

Drug-eluting cardiovascular stents are examples of coated medical devices that require controlled release of actives. Stents are used to treat atherosclerosis, where blood vessels are occluded by calcified lipid-laden plaque. Each year, over half a million tubular metal stents are implanted to provide mechanical support and restore adequate circulatory flow.[12] However, as many as 50% of patients who receive a bare-metal stent experience restenosis, where the blood vessel begins to renarrow due to excessive smooth muscle cell (SMC) proliferation that begins days after surgery and lasts for 3−4 weeks.[13,14] To combat this issue, drug-eluting stents were developed, which utilize a cytotoxic or immunosuppressive drug to suppress proliferation. Drug-eluting stents are commonly made of stainless steel or cobalt chrome and contain a base layer that promotes coating adhesion, a main layer for drug entrapment, and an overcoat to retard and extend drug release.[15] Sirolimus and paclitaxel are the most common drugs used to prevent the undesirable SMC proliferation, but

Special Issue: Biofunctional Biomaterials: The Third Generation of Medical Devices

Received: April 15, 2015
Revised: May 29, 2015
Published: June 4, 2015

DOI: 10.1021/acs.bioconjchem.5b00208
Bioconjugate Chem. 2015, 26, 1359−1369

these drugs and their polymer overcoats are associated with endothelial dysfunction, delayed healing, and hypersensitivity reactions, leading to reoccluded vessels, multiple surgeries, and potentially death.[16−18] Additionally, current active compounds do not address the upstream oxidative stress that triggers the restenosis cascade. As a result, patient mortality rates for drug-eluting stents are similar to those associated with bare-metal stents.[19] While there have been advances in alternative drugs and materials, most research has focused on drug mechanisms that reduce proliferation through cytotoxic or immunosuppressive approaches.

SAMs have been widely explored for implant coatings due to their ability to form ordered chains with facile fabrication, providing high grafting density and precisely controlled surface properties based on chemical structure. Further, SAMs have demonstrated good physical robustness through strong chemisorptions between thiols on gold,[3,20] silanes on silicon,[21,22] and phosphonic or alkanoic acids on metal oxides.[23−28] During organic acid self-assembly, anion(s) of alkanoic and phosphonic acids form coordination complexes between the surface's metal oxide cations, forming biocompatible, closely packed, and highly orientated molecular assemblies that can be applied to a wide range of metal oxide substrates.[24−26,29,30] Foster et al. evaluated the effect of headgroup functionality on grafting properties and demonstrated that alkyl phosphonic acids provide more ordered monolayers compared to alkyl carboxylic acids due to the close packing and relatively fewer packing defects.[31] One recent approach to fabricate alkanoic and phosphonic acid films is the tethering by aggregation and growth (T-BAG) method, which utilizes the molecular arrangement at the air−solvent interface to form self-assembled, ordered layers.[9,27,32,33] Subsequent annealing of the organized layers on the substrate results in robust chemisorbed layers that can withstand harsh chemical and mechanical conditions such as solvent-washing and peel tests.[25,32]

An alternative surface modification technique is the use of polymer brushes, which are polymer assemblies tethered to a surface or interface. While polymer brushes have similar properties to SAMs, the polymer chains form elongated conformations, allowing for thin films of tightly packed molecules. The majority of polymer brush coatings have been developed to minimize protein adsorption on implants.[34−41] Poly(ethylene glycol)- (PEG-) based polymer brush implant coatings, such as poly(L-lysine)−PEG, decrease SMC proliferation by at least 50% compared to bare-metal stents by reducing stent−cell interactions.[42,43] As polymer coatings are generally designed for permanent adsorption to limit protein interactions for the lifetime of the stent, few studies have focused on polymer-based coatings designed for extended release.[4,44]

The adsorption stability of various alkanoic and phosphonic acid-coordinated SAMs on a number of substrates have been evaluated in air, water, simulated body fluid, and buffer solutions.[25,26,45−48] While phosphonic acid layers formed by dip-coating were stable in air for at least 21 days, aqueous conditions drastically diminished the coating stability, leading to rapid desorption.[45] To provide stability in physiological conditions, Kaufman et al. used the T-BAG method with annealing and demonstrated that alkylphosphonic acids were stable for over 28 days in buffer.[47] The wide range of reported phosphonate SAM stability suggests that the phosphonate coating stability can be tailored to match physiological release requirements by varying the fabrication method or processing conditions.[49]

Recently, amphiphilic macromolecules (AMs), comprised of a hydrophilic PEG tail and a branched, sugar-based hydrophobic segment, were evaluated as restenosis therapeutics.[50] Carboxyl- and phosphonate-terminated AMs were effective in mediating SMC proliferation, thereby exhibiting the potential to limit vessel occlusion and the progression of restenosis. In a mechanism distinct from current cytotoxic or immunosuppressive drugs, AMs are designed to reduce proliferation through competitive inhibition of receptor-mediated oxidized low-density lipoprotein (oxLDL) uptake.[50] By mimicking key characteristics of oxidized lipids, AMs with the proper charge, hydrophobicity, three-dimensional conformation, and flexibility are able to effectively target SMC scavenger receptors and competitively inhibit oxLDL uptake.[51−60] In contrast to paclitaxel and sirolimus, AMs demonstrate superior cytocompatibility, demonstrating the potential to limit the strong immune response and locally toxic effects associated with drug-eluting stents.[53,56] AMs exhibit a concentration-dependent efficacy,[50] and thus, AM-based coatings must release a sufficient concentration to provide therapeutic benefits.

In this study, we hypothesize that AMs are capable of chemically adsorbing to metal oxides due to their headgroup functionalities and will be able to release, or desorb, from surfaces to provide bioactivity against SMC proliferation. As the headgroup functionality and linker lengths were previously found to affect the coating quality of small molecules,[23,31] this study evaluated the effect of headgroup functionality and linker length on macromolecular chemisorption and desorption to develop a controlled release coating that can suppress SMC proliferation. We synthesized one carboxyl- and two phosphonate-terminated macromolecules with varying alkane linker lengths (one or three methylenes preceding the terminal headgroup) and studied the chemical composition, thickness, grafting density, coating uniformity, bioactive AM release, and ability to reduce SMC proliferation. To the best of our knowledge, this work is the first time a macromolecular monolayer was designed to provide controlled release of the adsorbed bioactive amphiphile for a therapeutic effect.

RESULTS AND DISCUSSION

A series of bioactive AMs designed to reduce SMC proliferation were synthesized (Figure 1), where relevant parameters included the influence of terminal functionality (i.e., carboxyl vs phosphonate) and phosphonate linker length (i.e., methyl vs propyl) on the coating properties. AMs were subsequently immobilized on clean 316L stainless steel (SS316L) substrates via the T-BAG solution deposition method with heating to promote chemisorption. After monolayer formation, the film's chemical composition, thickness, wettability, uniformity, bioactive AM release, and ability to reduce SMC proliferation were quantified.

Synthesis. **1cM** and **Pr-1pM** were synthesized as previously published,[60,61] and **Me-1pM** was successfully synthesized in a similar manner (Scheme 1). Using a carbodiimide-mediated coupling reaction, *N*,*N*′-dicyclohexylcarbodiimide (DCC) and *N*-hydroxysuccinimide (NHS) were used to activate **1cM** before conjugating an aminophosphonic acid with triethylamine as the base. The activation of **1cM** was confirmed by the appearance of a singlet at 2.79 ppm in the proton nuclear magnetic resonance (^{1}H NMR) spectra, representative of the NHS methylene. Water was used as cosolvent for the coupling

DOI: 10.1021/acs.bioconjchem.5b00208
Bioconjugate Chem. 2015, 26, 1359−1369

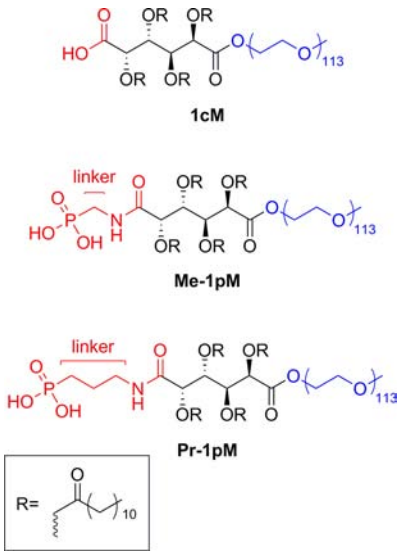

Figure 1. AMs with terminal carboxylate (**1cM**) or phosphonate (**Me-1pM**, **Pr-1pM**) headgroups (shown in red) have a sugar-based hydrophobic domain and a hydrophilic 5000 Da PEG domain.

of (aminomethyl) phosphonic acid due to limited solubility in tetrahydrofuran (THF). Disappearance of the NHS methylene peak and changes in mucate methine splitting was used to verify successful conjugation of (aminomethyl)phosphonic acid to **NHS-1cM**, due to the overlap between the methylene adjacent to the phosphonic acid and large PEG multiplet. **Me-1pM** was further characterized by gel permeation chromatography (GPC) to verify successful polymer synthesis.

Chemical Composition and Coverage. To confirm the chemical composition of coated monolayers, chemical states were determined by X-ray photoelectron spectroscopy (XPS, Table 1). From the survey spectra, the SS316L surface consisted primarily of Fe and Cr oxides and hydroxides. Relative to the SS316L reference surface, AM-coated samples showed significant increases in C 1s intensity and corresponding decreases in Fe 2p and Cr 2p intensities, suggesting AM adsorption (Table 2). The overlaid C 1s core spectra (Figure 2) demonstrate distinct aliphatic (C–C/C–H), ether (C–O), and ester/amide (O=C–O/O=C–N) functional groups in the AM structures. All AM-coated samples contained high levels of the C 1s C–O–C and O 1s C–O–C peaks, indicating the presence of PEG chains on the surface. The O 1s core spectra for each sample were also recorded (Supporting Information, Figure S1), but the amide, ester, ether, and carbonyl peaks in the AM-coated samples obscure the phosphonate's P=O, P–O–Fe, and P–O–H peaks, making it difficult to discern the ratios between attached P–O–Fe and unattached P–O–H and P=O to confirm the covalent attachment of phosphonate molecules on the oxide surface. As a result, the overall O 1s peak intensities were used to qualitatively compare AM-coated samples and the uncoated SS316L control, where increased amide, ester, hydroxyl, and ether peak intensities on AM-coated surfaces compared to bare SS316L suggest successful surface attachment (Supporting Information, Figure S1). Lastly, the unique presence of P 2p signal for phosphonate-based SAMs suggests successful chemisorptions. The corresponding binding energies of P 2p signals are indicative of coordination between the phosphonate headgroups and the metal oxide surface. The presence of these signals after the multiple rinse steps during preparation indicates strong coordination between AMs and the substrate.

As the AM bioactivity is concentration-dependent, high surface coverage corresponding to high bioactive loading is desirable to reduce SMC proliferation. A large scan area of 400 × 400 μm^2 was used to evaluate the AMs' coverage on SS316L substrates. The component ratios illustrate differences between AM adlayers. In particular, higher C/Fe ratios for **1cM** and **Pr-1pM** adlayers demonstrate greater surface coverage compared to **Me-1pM** adlayers. Additionally, the decreased O/C ratio of all AM coatings indicates reduced amounts of surface oxide and hydroxide compared to bare SS316L, demonstrating that AM molecules displace surface oxides and hydroxides. The O/C values obtained in these experiments (0.85–0.93) are consistent with previously reported O/C ratios for PEG-grafted surfaces, further confirming the successful adsorption of AMs.[62]

Finally, a difference in the P/Fe ratio between the two phosphonate AMs was observed, suggesting that linker length influences the coating quality. Specifically, **Pr-1pM** exhibited an increased P/Fe ratio compared to **Me-1pM**; these data indicate that **Pr-1pM** forms high monolayers with high surface coverage and thus higher bioactive loading on the substrate as compared to **Me-1pM**.

Thickness and Grafting Density. As AM bioactivity is concentration-dependent,[50] greater bioactive AM loading on the stent surface is desirable to suppress SMC proliferation. Thus, the grafting density of the films was compared using ellipsometry measurements. The experimental dry thickness was determined to be between 2.8 and 3.4 nm, depending on the adsorbed AM (Table 3). The sample thickness is largely attributed to the large size of the 5000 Da PEG tail. The dry thickness values are in the range of those reported for 5000 Da PEG–thiol layers on gold (~2.9 nm), and 5000 Da PEG–catechol layers on titanium (~2.4–3.2 nm).[36,63]

According to Sofia et al., the grafting density can be modeled based on the dry thickness values obtained by ellipsometry.[40,64] Assuming a uniformly grafted layer, the grafting density (σ) is given by the equation:

Scheme 1. Synthetic Scheme of Me-1pM from Previously Synthesized 1cM

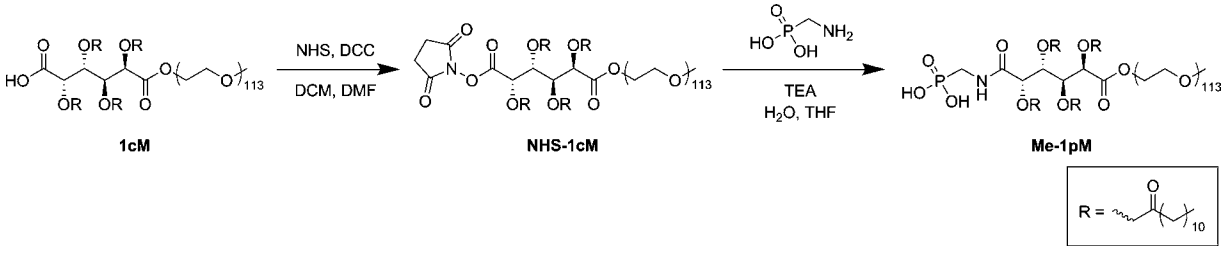

DOI: 10.1021/acs.bioconjchem.5b00208
Bioconjugate Chem. 2015, 26, 1359–1369

Table 1. XPS Binding Energies and Fitting Parameters

element	assignment	binding energy (eV)	full width at half-maximum (eV)
C 1s	C–C/C–H	285.0	1.63 ± 0.04
	C–O–C/C–P/C–N	286.6	1.63 ± 0.04
	O=C–O/O=C–N	289.2	1.63 ± 0.04
O 1s	Fe–O/Cr–O	530.2 ± 0.1	1.52 ± 0.01
	Fe–O–H/C–O–Fe/P–O–Fe/P=O	531.8 ± 0.1	1.52 ± 0.01
	C–O–C/C=O	532.8 ± 0.1	1.95 ± 0.03
	C–O–C=O/NH–C–O/C–O–H/P–O–H	533.7 ± 0.1	1.62 ± 0.05
P 2p	P $2p_{3/2}$	133.3 ± 0.1	1.75 ± 0.07
	P $2p_{1/2}$	134.2 ± 0.1	1.75 ± 0.07
Cr 2p	Cr $2p_{3/2}$	576.7 ± 0.1	3.47 ± 0.05
	Cr $2p_{1/2}$	586.6 ± 0.1	2.88 ± 0.04
Fe 2p	Fe $2p_{3/2}$	710.8 ± 0.1	2.97 ± 0.05
		715.3 ± 0.1	6.72 ± 0.28
	Fe $2p_{1/2}$	724.3 ± 0.1	2.88 ± 0.04
		733.0 ± 0.1	4.53 ± 0.22

Table 2. Chemical Composition of AM Adlayers

	atomic concentration (%)					component ratios		
sample	C 1s	O 1s	P 2p	Cr 2p	Fe 2p	C/Fe	O/C	P/Fe
SS316L	13.03	57.95	0.28	1.18	27.55	0.47	4.45	0.01
1cM	51.15	45.15	0.20	0.26	3.57	14.33	0.88	0.06
Me-1pM	47.40	44.23	1.23	0.51	6.61	7.17	0.93	0.19
Pr-1pM	50.54	42.78	1.94	0.27	4.47	11.31	0.85	0.43

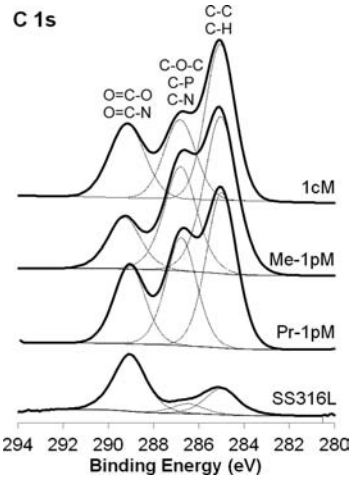

Figure 2. High resolution C 1s core spectra demonstrate significant changes in ether and ester/amide peak intensities on AM-coated surfaces compared to bare SS316L.

Table 3. Ellipsometric Thickness and Theoretical Grafting Density

sample	thickness (nm)	theoretical molecular area (nm^2)	theoretical grafting density (chains/nm^2)
1cM	3.3 ± 0.1	2.7	0.37
Me-1pM	2.8 ± 0.1	3.3	0.30
Pr-1pM	3.4 ± 0.1	2.7	0.37

$$\sigma = \frac{1}{L^2} = \frac{d\rho N_A}{M}$$

where L^2 is the theoretical molecular area occupied by an AM chain, d is the film thickness, ρ is the bulk density of PEG (~1.17 g/mL),[64] N_A is Avogadro's number, and M is the AM molecular weight. The calculated molecular area and grafting density are shown in Table 3. While **1cM** and **Pr-1pM** chains occupied a similar molecular area and had similar grafting densities, **Me-1pM** was less densely coated, suggesting a decreased bioactive AM loading capacity.

Coating Uniformity Evaluated by Dynamic Contact Angle Goniometry and AFM. Studies have shown that rough stent surfaces may induce vascular SMC proliferation.[65] Dynamic contact angle measurements were recorded to understand the hysteresis, where differences in advancing and receding contact angles are an indication of the sample roughness and homogeneity.[66,67] AM-coated samples exhibit advancing aqueous contact angles ranging from 31° to 45°, depending on the headgroup, and receding contact angles of approximately 27°. The lower advancing contact angle of the adsorbed AMs compared to SS316L suggests AM attachment and hydrophilic PEG presentation as the terminal group (Table 4).[66] The lower hysteresis of **1cM** and **Pr-1pM** as compared to **Me-1pM** also suggests a smoother and more homogeneous layer, which is advantageous for stent coating applications. Additionally, **Me-1pM** demonstrated higher advancing contact angles, which may be due to the water drop contacting either exposed AM hydrophobic domains or the SS316L substrate. Lastly, the differences in hydrophilicity correspond with

DOI: 10.1021/acs.bioconjchem.5b00208
Bioconjugate Chem. 2015, 26, 1359–1369

Table 4. Dynamic Contact Angle Measurements

sample	advancing	receding	hysteresis
SS316L	74 ± 0	54 ± 1	20
1cM	32 ± 1	28 ± 2	4
Me-1pM	45 ± 3	27 ± 1	18
Pr-1pM	31 ± 1	27 ± 2	4

differences in dry thickness between samples. Generally, thicker samples as determined by ellipsometry measurements also have lower hysteresis values. These results suggest that the two AMs (**1cM** and **Pr-1pM**) are more densely coated on the substrate and more homogeneous than **Me-1pM** coatings.

The coating surface morphology was also evaluated by AFM to provide further homogeneity characterization to confirm the contact angle results. The images demonstrate uniformly spaced AMs (Figure 3) with a height of approximately 3.5

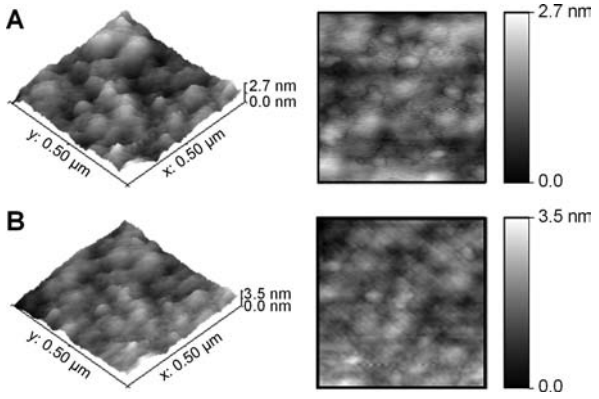

Figure 3. AFM morphology demonstrates uniformly spaced **Pr-1pM** molecules.

nm. Together with the contact angle data, the AFM images suggest that **Me-1pM** molecules have a different conformation on the surface compared to **1cM** and **Pr-1pM** molecules. Specifically, **Me-1pM** coatings were thinner, with a lower grafting density. As the hydrophobic domain and PEG in all AM systems were identical, it is likely that the linker influences AM adsorption properties.

Proposed Molecular Adsorption Characteristics. Understanding the AM molecular arrangement as well as the intramolecular and intermolecular forces on the surface can provide insight into the data obtained for this work to rationally design the next generation of AM coatings. While additional studies are needed to elucidate the precise conformation on the surface, a theoretical discussion below is based on adsorption results and theory of surface forces.

In traditional SAM formation by dip-coating, an initial adsorption occurs within minutes, followed by slow molecular rearrangement over a period of approximately 24 h to maximize the van der Waals forces between chains.[68] With the T-BAG method, molecules are arranged at the gas−liquid interface, promoting well-organized layer formation as the solvent evaporates.[69,70] If the PEG chain forms a coil in solution, the coating is likely to form with the PEG chain in mushroom conformation, as high grafting density and very specific thermodynamic driving forces are required for PEG to elongate into brush-like structures on the surface.[34,63,71−73]

A proposed structural model was developed to provide a graphical representation of the potential surface chain structure (Figure 4), in which PEG forms a distinct layer clearly separated from the hydrophobic layer.[74] Although the figure

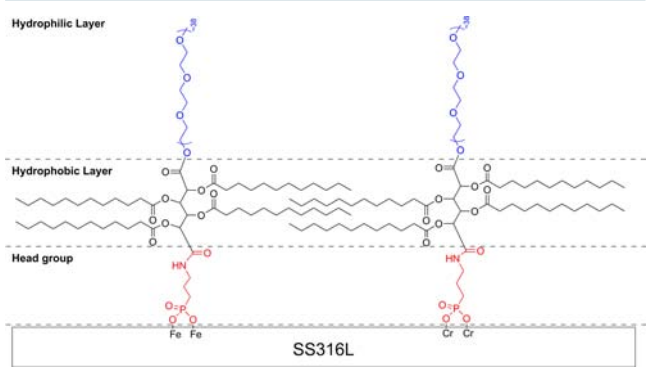

Figure 4. Proposed model of the macromolecular organization of **Pr-1pM** on SS316L substrates.

represents a simplified model, in reality, the hydrophobic lauroyl side arms likely adopt a nonlinear folded or entangled conformation to maximize van der Waals interactions. Additional studies using angle-resolved XPS or with a surface forces apparatus are necessary to further investigate this phenomena.[75]

For small molecule adsorption, previous studies evaluating the effect of headgroup chemistry demonstrate that phosphonates generally have stronger adsorption than carboxylates over a range of alkyl chain lengths. However, we observe that for AMs, variations in the phosphonate linker length have a more significant influence on adsorption than variations between headgroups. Uniquely, the phosphonic acid AM linkers contain an aliphatic segment connected to the remainder of the AM structure through an amide bond. The presence of the amide allows for potential intramolecular hydrogen bonding to occur between the amide and phosphonate oxygen atoms, resulting in cyclic structure. The ring conformation would be more entropically favored for **Me-1pM** than **Pr-1pM**, as a 5- or 6-membered ring is more likely to form than a 7-membered ring. This ring may limit the availability of one of the coordinating phosphonate oxygen atoms for surface binding, thus decreasing the likelihood of bi- or tridentate binding. The grafting density and monolayer thickness of **Pr-1pM** and **1cM** are likely similar because **Pr-1pM** is less likely to form a constrained ring and **1cM** is unable to form a ring, leaving more phosphonate oxygen atoms available to coordinate to surface.

AM Coatings Release In a Controlled Manner. While traditional SAMs are often used to provide a stable interface to permanently influence a substrate's properties, AM coatings are designed to deliver bioactives over time. To relate the release profiles with the timing of physiological events, a continuous aqueous flow test was conducted to measure the AM release from SS316L surfaces under simulated shear stress conditions that occur in a physiological environment. In these experiments, 4-(2-hydroxyethyl)-1-piperazineethanesulfonic acid (HEPES) buffer was used, as phosphate buffered saline has previously demonstrated competitive surface binding effects.[48,76]

In vitro bioactive AM release studies via QCM-D reveal significant differences in the release profiles of the AMs, indicating that the coatings have varying levels of stability. **Me-1pM** demonstrated nearly complete release (~96% cumulative release) in 7 days. Defects in monolayer organization act as a primary mode of instability, as water competes to bind with the surface at a defect site.[45,77] Given that phosphonic acids

DOI: 10.1021/acs.bioconjchem.5b00208
Bioconjugate Chem. 2015, 26, 1359−1369

typically exhibit strong chemisorption to metal oxides,[31,32] it is hypothesized that the fast release of **Me-1pM** as compared to the **1cM** and **Pr-1pM** coatings may be due to the weaker coordination associated with monodentate binding and lower grafting density, which allows water to penetrate the coating and compete for surface binding (Figure 5).[45,47] As the AM

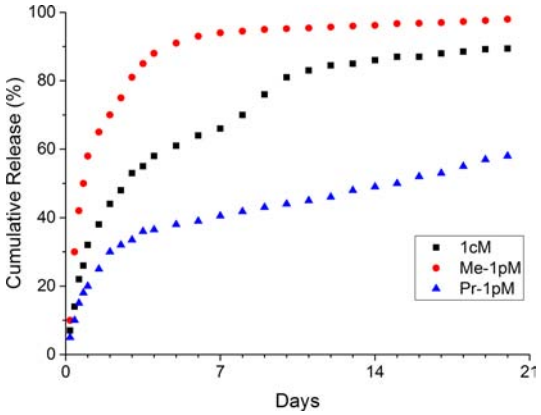

Figure 5. Release profiles of AM adlayers in HEPES buffer demonstrate varying levels of stability, where **Me-1pM** desorbed in a burst release over 7 days, but **1cM** and **Pr-1pM** coatings demonstrated sustained release over 21 days.

hydrophobic domain is extremely nonpolar, densely packed AMs, such as **1cM** and **Pr-1pM**, may shield the AM headgroup from water penetration in aqueous conditions for the proposed model in Figure 4.

In comparing headgroups, **1cM** and **Pr-1pM** resulted in extended release of the bioactive from the substrate surface. For both coatings, a burst release of approximately 30% for **Pr-1pM** and 60% for **1cM** was observed, followed by continuous sustained release. Kaufman and co-workers also showed a fast initial desorption with continued sustained release for phosphonate SAMs on SS316L substrates and proposed that the mechanisms for degradation are hydrolytic cleavage at the headgroup driven by mixed binding modes and packing defects associated with small molecule monolayers.[47] Molecules weakly attached by van der Waals interactions desorb quickly, but strongly bound molecules coordinated to the surface desorb over time. Thus, in comparing **Pr-1pM** and **1cM** coatings, the data suggests that **Pr-1pM** is more strongly bound to the surface as compared to **1cM**, which is consistent with previous findings that phosphonates generally form more robust coordination bonds to aluminum oxide than carboxylates.[31]

Notably, **1cM** demonstrates a biphasic release profile, with rapid initial release during the first 5 days that gradually slows before a second rapid release around the ninth day. The dual-phase release profile may be due to mixed monodentate and bidentate binding modes, where the monodentate bound AMs are hydrolytically cleaved in the initial fast release, followed by the bidentate bound molecules in the second rapid release.[26] In contrast, **Pr-1pM** demonstrated an initial rapid release followed by steady gradual desorption over 28 days, suggesting that **Pr-1pM** molecules are bound to the surface through multidentate coordination.[25] **Pr-1pM** has extended stability, as do previously reported short chain phosphonates on SS316L.[47] However, time-dependent release studies comparing **Pr-1pM** and alternative amphiphilic PEG systems should be conducted to assess the influence of the hydrophobic layer on preventing water penetration, thus limiting the hydrolytic-mediated release observed in other studies.[45,47]

AM Coatings Suppress SMC Proliferation. The restenosis cascade begins with platelet aggregation and inflammation directly after stent implantation, uncontrolled oxidative stress that causes SMC proliferation for four or more weeks.[13] To match restenosis events, controlled release coatings were developed to provide bioactivity over the course of the SMC proliferative phase to prevent vessel reocclusion in restenosis. AM coatings were evaluated in serum-free conditions to isolate the effects of oxLDL-induced proliferation,[78] as serum conditions have previously been shown to induce SMC proliferation.[79] In the experimental design, SMCs were coincubated for 24 h with oxLDL and AM eluent from the QCM release experiments collected on days 1, 3, 7, 14, or 21. Proliferation was quantified by cellular DNA content using the fluorescence-based CyQUANT assay to determine the number of cells as a percentage of the oxLDL-only control. While **1cM**, **Me-1pM**, and **Pr-1pM** all demonstrate a significant reduction in oxLDL-induced SMC proliferation over 14 days, they affected SMC proliferation to varying extents at each time point (Figure 6). After 1 day, **Me-1pM** initially reduced SMC

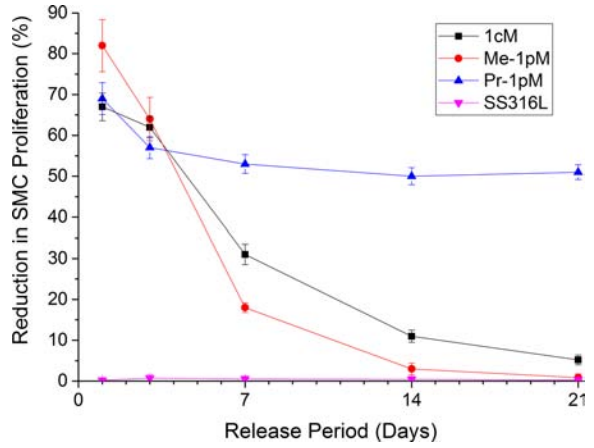

Figure 6. AM coatings significantly reduce levels of SMC proliferation after 24 h cotreatments of oxLDL and release media. **1cM**, **Me-1pM**, and **Pr-1pM** adlayers reduce SMC proliferation by up to 80% initially, with **Pr-1pM** providing continued suppression of SMC proliferation over 21 days.

proliferation to a significant amount (82%) compared to the oxLDL-only control but demonstrated only minor improvements at 14 days. **1cM** also provided significant reduction in SMC proliferation in the first 3 days, but this efficacy also decreased over 14 days. In contrast, **Pr-1pM** coatings exhibited gradual release that maintained at least 50% reduction in SMC proliferation throughout the study. These findings also generally correspond with the amount of AMs in the release media, which is consistent with a previous study evaluating the AM concentration-dependent effects on SMC proliferation.[50] Thus, **Pr-1pM** demonstrates the most suitable characteristics for the stent coating.

As the cytotoxic and/or immunosuppressive mechanisms employed by current drug-eluting stents are associated with delayed endothelial healing, the cytotoxicity of AM treatments was assessed. SMCs treated with AMs from the release eluent demonstrated high cell viability (Supporting Information, Figure S2). These results indicate that AM treatments are

DOI: 10.1021/acs.bioconjchem.5b00208
Bioconjugate Chem. 2015, 26, 1359−1369

able to reduce SMC proliferation with low associated cytotoxicity, which differentiates AM coatings from clinically approved stent technologies.

Although the restenosis cascade is heavily driven by SMC hyperproliferation, other cell types are also involved. Current drug-eluting stents cause endothelial dysfunction, as the stent expansion damages the vessel lining and the cytotoxic or immunosuppressive drugs prevent endothelial cells from healing. As AMs limit SMC proliferation using a noncytotoxic approach, it is expected that damaged endothelial cells will be able to efficiently heal. Collaborative studies conducted with the Moghe group have demonstrated that endothelial cells treated with AMs for 24 h have good cell viability (~96% viability relative to basal control), suggesting that AM treatments will not negatively impact endothelial healing.[80,81] Additionally, the AMs reduce oxLDL uptake, thereby limiting the possibility of excessive oxLDL-induced endothelial proliferation, which can also lead to restenosis.[80−82]

CONCLUSION

Although restenosis is a common issue with bare-metal stents, drug-eluting stent coatings are associated with endothelial dysfunction, delayed healing, and hypersensitivity reactions, leading to reoccluded vessels, multiple surgeries, and possibly patient mortality.[16−18] In this study, we developed self-assembled AMs that gradually release from metal oxide surfaces to suppress SMC proliferation. AM adlayers with carboxyl or phosphonate headgroups were coated on SS316L using the T-BAG approach to study the effect of headgroup functionality on the coating composition, thickness, grafting density, and uniformity. Subsequent characterization suggests high grafting density of **1cM** and **Pr-1pM**. On the other hand, adsorption characterization data regarding **Me-1pM** demonstrate lower grafting density that ultimately correlates with faster release and reduced suppression of SMC proliferation after 3 days. In contrast to previous studies where carboxylates demonstrated weak adsorption, we observed that **1cM** demonstrates high grafting density and good stability in physiological conditions, suggesting the ability for a controlled release of coated macromolecules. Moreover, **Pr-1pM** coatings were uniform, with high grafting density and delayed release. Overall, **1pM** demonstrated significant reductions in SMC proliferation over 21 days, consistent with release characteristics. These results, in addition to the low associated cytotoxicity, demonstrates the potential of AM controlled release coatings for medical device applications.

EXPERIMENTAL SECTION

Materials. Reagents were purchased from Sigma-Aldrich (Milwaukee, WI) and used without further purification unless otherwise mentioned. PEG methyl ether (M_n = 5000 Da) was azeotropically distilled with toluene prior to use. 316L stainless steel foil sheets (0.50 mm, 99.99%) were purchased from Goodfellow Inc. (Coraopolis, PA). Ultrapure water (18.2 MΩ), obtained using a PicoPure 2 UV Plus system (Hydro Service and Supplies, Durham, NC), was used for all studies. Buffer for release studies was prepared by dissolving 10 mM HEPES and 150 mM sodium chloride in deionized ultrapure water, and pH was adjusted to 7.4 with 1 N sodium hydroxide, then filtered with a 0.2 μm nylon filter before use. Human primary coronary artery SMCs, Smooth Muscle Basal Media (SmBM), and Smooth Muscle Growth Media-2 SingleQuots were purchased from Lonza (Walkersville, MD), unlabeled oxLDL was purchased from Biomedical Technologies Inc. (Ward Hill, MA), Falcon T75 flasks were purchased from BD Biosciences (San Jose, CA), and a CyQUANT NF Cell Proliferation Assay Kit was purchased from Life Technologies (Carlsbad, CA).

AM Synthesis and Characterization. **1cM** and **Pr-1pM** were synthesized as previously described.[60,61] **Me-1pM** was prepared following a modified procedure of the previously synthesized **Pr-1pM** (Scheme 1). In brief, **1cM** (1.60 g, 0.26 mmol) was first activated by NHS (0.19 g, 0.42 mmol) in anhydrous dichloromethane (DCM, 7 mL) at room temperature for 24 h with DCC (1 M in DCM, 0.40 mmol) as the coupling reagent. An NHS-activated 1cM intermediate (**NHS-1cM**) was yielded as a white power (1.3 g, 80%).

To then synthesize **Me-1pM**, (aminomethyl) phosphonic acid (0.20 g, 0.17 mmol) was dissolved in high-performance liquid chromatography (HPLC) grade water (1.3 mL) at 37 °C and cooled to room temperature upon complete dissolution. HPLC grade THF(2.0 mL) and triethylamine (TEA, 0.086 mL, 0.62 mmol) were then added to the reaction flask under stirring. In a separate vial, **NHS-1cM** (0.25 g, 0.041 mmol) was dissolved in HPLC grade THF (6 mL), and the mixture transferred to the reaction flask. The resulting yellow solution was stirred for 18 h. THF was removed in vacuo, and the resulting yellow oil reconstituted in DCM (15 mL) and washed with 0.1 N hydrochloric acid (HCl, 30 mL) for 30 min. The mixture was washed with 0.1 N HCl (1 × 30 mL) and 50:50 brine/H_2O (2 × 30 mL). The organic layer was dried over magnesium sulfate ($MgSO_4$) and concentrated in vacuo. Crude product was dissolved in minimal DCM (5 mL) and 10-fold diethyl ether added, resulting in the precipitation of **Me-1pM**. **Me-1pM** was isolated via centrifugation at 3500 rpm for 5 min and decanting the supernatant. The product was washed with diethyl ether (50 mL × 3) and isolated via centrifugation. **Me-1pM** was obtained as a white waxy solid (0.061 g, 24%).

AM chemical structures were confirmed by ^{1}H NMR spectroscopy recorded on a Varian 400 MHz spectrophotometer. AMs (~5 mg/mL) were dissolved in deuterated chloroform ($CDCl_3$) with tetramethylsilane (TMS) as an internal reference. Molecular weights (M_w) and polydispersity indices (PDI) were determined by GPC on a Waters LC system equipped with a PLgel MIXED column and a 2414 refractive index detector. HPLC grade DCM was used as the solvent for sample preparation and eluent for analysis. Samples (10 mg/mL) were prepared in DCM and filtered through 0.45 μm polytetrafluoroethylene (PTFE) syringe filters prior to injection at a flow rate of 1.0 mL/min. Broad molecular weight PEG standards (Waters, Milford, MA) were used for calibration. WaterBreeze v3.20 software was used for data collection and processing.

^{1}H NMR (400 MHz, $CDCl_3$): δ = 5.17−5.74 (m, 4H, CH), 3.64 (m, ~500H, CH_2CH_2O), 3.38 (s, 3H, CH_3), 2.42 (t, 4H, CH_2CO), 2.28 (t, 4H, CH_2CO), 1.61 (t, 4H, CH_2CO), 1.52 (t, 4H, CH_2CO), 1.25 (m, 64H, CH_2). M_w = 8.2 kDa; PDI = 1.1.

Stainless Steel Substrate Preparation. SS316L foil sheets (0.50 mm, 99.99%) were cut into 10 mm × 30 mm coupons and polished with 240, 600, and 1200 grit silicon carbide paper, rinsed, and cleaned by ultrasonication in methanol (2 × 15 min), followed by immersion in boiling methanol for 1 h to remove contaminants. Cleaned samples were dried under a stream of 0.2 μm-filtered nitrogen and exposed to ultraviolet light and ozone for 30 min (UVO-Cleaner 42, Jelight Company Inc., Irvine, CA).

DOI: 10.1021/acs.bioconjchem.5b00208
Bioconjugate Chem. 2015, 26, 1359−1369

SAM Formation. Substrates were coated using the T-BAG method, as previously described.[33] Briefly, cleaned substrates were submerged in 0.15 mM solution of **1cM**, **Me-1pM**, or **Pr-1pM** in anhydrous DCM. The solvent was allowed to evaporate until the liquid level was below the substrate, after which time the substrates were dried at 140 °C for 48 h, rinsed with DCM (2 × 30 mL), and dried under a stream of nitrogen. Samples were prepared in triplicate and used immediately after preparation.

Spectroscopic Ellipsometry. Ellipsometry measurements were performed on a Jobin Yvon UVISEL spectroscopic ellipsometer (Horiba Scientific, Irvine, CA) in the spectral range of 370−1000 nm with a 70° angle of incidence. Measurements were recorded under ambient conditions immediately pre- and postmonolayer formation. The measured phase difference (Δ) and amplitude component (Ψ) data was fit with a Cauchy model (A_n = 1.45, B_n = 0.01 μm^2, C_n = 0.00) in the integrated Horiba DeltaPsi2 software to obtain ellipsometric thickness.[83] Results are the mean of measurements recorded on three distinct locations on each of three independent samples.

X-ray Photoelectron Spectroscopy. XPS data were recorded using a Thermo Scientific K-Alpha (Waltham, MA) instrument configured with a monochromatic Al Kα radiation source (1486.6 eV) and a flood gun for charge compensation. Measurements were recorded over a scan area of 400 μm at a 45° takeoff angle and 90° emission angle under ultra high vacuum conditions (pressure <5 × 10^{-9} mbar). Broad survey scans were taken at pass energies of 200 eV, and detailed core scans were taken at pass energies of 50 eV. All binding energies were referenced to the aliphatic C−C/C−H C 1s component at 285.0 eV. XPS spectra were analyzed using the integrated Thermo Avantage software. High resolution core spectra (P 2p, C 1s, Cr 2p, Fe 2p, O 1s) were deconvoluted into their components by subtracting Shirley backgrounds and fitting Gaussian−Lorentzian functions and least-squares-fit routines to the core level features. Results are the mean of measurements recorded on three independent samples. The fitting parameters are summarized in Table 1.

Dynamic Contact Angle Goniometry. Advancing and receding contact angles were measured in a VCA Optima system (AST Products, Inc., Billerica, MA) using an aqueous sessile drop experiment. The drop size was mechanically increased and decreased at a speed of 15 μL/min. Results are the mean of measurements recorded on three distinct locations on each of three independent samples.

Atomic Force Microscopy (AFM). Film morphology images were obtained with a NanoScope IV AFM (Digital Instruments-Veeco, Santa Barbara, CA) in tapping mode with silicon tips with a spring constant of 50 N/m according to established procedures.[84] Images were recorded from three independent samples.

Quantification of Bioactive AM Release. Because of the low absorptivity of AM molecules in the ultraviolet and visible range, AM release from the substrate surface was assessed by mass loss using quartz crystal microbalance with dissipation (QCM-D). Stainless steel quartz sensors (Biolin Scientific, Stockholm, Sweden) were coated using the AM self-assembly procedure described above. Changes in frequency and dissipation were monitored in situ in a Q-Sense E4 QCM-D (Biolin Scientific, Stockholm, Sweden) equilibrated with 37 °C HEPES buffer flowing at a continuous rate of 0.96 μL/min generated by a Ismatec IPC-N peristaltic pump (Cole Parmer, Vernon Hills, IL). Frequency was recorded for overtones n = 3, 5, and 7. The change in mass per area was obtained using a Voigt viscoelastic model. Results are the mean of measurements recorded on three independent samples. At the conclusion of the study, preservation of the AM chemical structure in release media was confirmed by ^{1}H NMR, as described above.

Smooth Muscle Cell Culture and Proliferation Assay. SMC culture was conducted as previously described.[50] Briefly, human primary coronary artery SMCs between passages 3−6 were cultured in SmBM supplemented with 5% fetal bovine serum (FBS) and Smooth Muscle Growth Media-2 SingleQuots and maintained in unmodified T75 flasks at 37 °C in a humidified atmosphere containing 5% CO_2. Media was changed every 2 days until cells were passaged (~80% confluency).

For the proliferation assay, cells were plated in an unmodified 96-well plate at a seeding density of 5000 cells/cm^2 and allowed to rest in serum-free SmBM for 24 h to induce cell quiescence. After 24 h, the media was aspirated and replaced with sterile-filtered cotreatments. The treatments were prepared by adding 10 μg/mL of oxLDL to AMs in the release buffer collected on days 0, 1, 3, 7, and 14 of the QCM-D release experiment (1:3 dilution of release stock in serum-free SmBM). After a 24 h incubation, cell proliferation was assessed using a CyQUANT NF Cell Proliferation Assay Kit following the manufacturer's protocol, which measures cellular DNA content via fluorescent dye binding to count the number of cells. Results are the mean of three independent experiments with two technical replicates per experiment.

Statistical Analysis. Statistical analyses were performed using JMP software by SAS. Statistical significance ($p \leq 0.05$) was determined using a one-way ANOVA with Tukey's posthoc test for comparisons between multiple groups.

■ ASSOCIATED CONTENT

Supporting Information

XPS O 1s core spectra and cell viability results. The Supporting Information is available free of charge on the ACS Publications website at DOI: 10.1021/acs.bioconjchem.5b00208.

■ AUTHOR INFORMATION

Corresponding Author

*E-mail: keuhrich@rutgers.edu.

Notes

The authors declare no competing financial interest.

■ ACKNOWLEDGMENTS

We gratefully acknowledge Bahar Demirdirek and Amy Huang for technical assistance and Dr. Sanjeeva Murthy, Dr. Vinod Damodaran, and Alysha Moretti for scientific discussions. We also thank Dr. Gene Hall and Dr. Dunbar Birnie for access to equipment. This work was supported with funding provided by the National Institutes of Health (NIH R01 HL107913) and the National Science Foundation Graduate Research Fellowship (NSF DGE-1433187) awarded to J.W.C.

■ REFERENCES

(1) Santin, M., Morris, C., Harrison, M., Mikhalovska, L., Lloyd, A., and Mikhalovsky, S. (2004) Factors inducing in-stent restenosis: an in vitro model. *Med. J. Malaysia 59*, 93−94.

(2) Ulman, A. (1996) Formation and structure of self-assembled monolayers. *Chem. Rev. 96*, 1533−1554.

DOI: 10.1021/acs.bioconjchem.5b00208
Bioconjugate Chem. 2015, 26, 1359−1369

(3) Love, J. C., Estroff, L. A., Kriebel, J. K., Nuzzo, R. G., and Whitesides, G. M. (2005) Self-assembled monolayers of thiolates on metals as a form of nanotechnology. *Chem. Rev. 105*, 1103−1170.
(4) Mani, G., Torres, N., and Oh, S. (2011) Paclitaxel delivery from cobalt−chromium alloy surfaces using self-assembled monolayers. *Biointerphases 6*, 33−42.
(5) Ding, N. and Helmus, M. N. (2000) Medical devices with long term non-thrombogenic coatings. Patent US 6120536 A, Schneider Inc..
(6) Chrisey, L. A., Lee, G. U., and O'Ferrall, C. E. (1996) Covalent attachment of synthetic DNA to self-assembled monolayer films. *Nucleic Acids Res. 24*, 3031−3039.
(7) Bamdad, C. (1998) A DNA self-assembled monolayer for the specific attachment of unmodified double-or single-stranded DNA. *Biophys. J. 75*, 1997−2003.
(8) Rezania, A., Johnson, R., Lefkow, A. R., and Healy, K. E. (1999) Bioactivation of metal oxide surfaces. 1. Surface characterization and cell response. *Langmuir 15*, 6931−6939.
(9) Gawalt, E. S., Avaltroni, M. J., Danahy, M. P., Silverman, B. M., Hanson, E. L., Midwood, K. S., Schwarzbauer, J. E., and Schwartz, J. (2003) Bonding organics to Ti alloys: facilitating human osteoblast attachment and spreading on surgical implant materials. *Langmuir 19*, 200−204.
(10) Ostuni, E., Chapman, R. G., Liang, M. N., Meluleni, G., Pier, G., Ingber, D. E., and Whitesides, G. M. (2001) Self-assembled monolayers that resist the adsorption of proteins and the adhesion of bacterial and mammalian cells. *Langmuir 17*, 6336−6343.
(11) Pallavicini, P., Taglietti, A., Dacarro, G., Diaz-Fernandez, Y. A., Galli, M., Grisoli, P., Patrini, M., De Magistris, G. S., and Zanoni, R. (2010) Self-assembled monolayers of silver nanoparticles firmly grafted on glass surfaces: low Ag^+ release for an efficient antibacterial activity. *J. Colloid Interface Sci. 350*, 110−116.
(12) Lloyd-Jones, D., et al. (2009) Heart disease and stroke statistics 2009 update: a report from the American Heart Association Statistics Committee and Stroke Statistics Subcommittee. *Circulation 119*, 480−486.
(13) Kenagy, R. (2011) Biology of Restenosis and Targets for Intervention. In *Mechanisms of Vascular Disease* (Fitridge, R., and Thompson, M., Eds.) pp 115−151, University of Adelaide Bar Smith Press, Adelaide, Australia.
(14) Serruys, P. W., et al. (2001) Comparison of coronary-artery bypass surgery and stenting for the treatment of multivessel disease. *N. Engl. J. Med. 344*, 1117−1124.
(15) Puranik, A. S., Dawson, E. R., and Peppas, N. A. (2013) Recent advances in drug eluting stents. *Int. J. Pharm. 441*, 665−679.
(16) Inoue, T., Croce, K., Morooka, T., Sakuma, M., Node, K., and Simon, D. I. (2011) Vascular inflammation and repair implications for re-endothelialization, restenosis, and stent thrombosis. *JACC Cardiovasc. Interv. 4*, 1057−1066.
(17) Otsuka, Y., Chronos, N., Apkarian, R. P., and Robinson, K. A. (2007) Scanning electron microscopic analysis of defects in polymer coatings of three commercially available stents: Comparison of BiodivYsio, Taxus and Cypher stents. *J. Invasive Cardiol. 19*, 71−76.
(18) Virmani, R., Guagliumi, G., Farb, A., Musumeci, G., Grieco, N., Motta, T., Mihalcsik, L., Tespili, M., Valsecchi, O., and Kolodgie, F. D. (2004) Localized hypersensitivity and late coronary thrombosis secondary to a sirolimus-eluting stent: should we be cautious? *Circulation 109*, 701−705.
(19) Mitra, A., and Agrawal, D. (2006) In stent restenosis: bane of the stent era. *J. Clin. Pathol. 59*, 232−239.
(20) Bain, C. D., Troughton, E. B., Tao, Y. T., Evall, J., Whitesides, G. M., and Nuzzo, R. G. (1989) Formation of monolayer films by the spontaneous assembly of organic thiols from solution onto gold. *J. Am. Chem. Soc. 111*, 321−335.
(21) Toworfe, G., Composto, R., Shapiro, I., and Ducheyne, P. (2006) Nucleation and growth of calcium phosphate on amine-, carboxyl- and hydroxyl-silane self-assembled monolayers. *Biomaterials 27*, 631−642.
(22) Haensch, C., Hoeppener, S., and Schubert, U. S. (2010) Chemical modification of self-assembled silane based monolayers by surface reactions. *Chem. Soc. Rev. 39*, 2323−2334.
(23) Spori, D. M., Venkataraman, N. V., Tosatti, S. G., Durmaz, F., Spencer, N. D., and Zürcher, S. (2007) Influence of alkyl chain length on phosphate self-assembled monolayers. *Langmuir 23*, 8053−8060.
(24) Tosatti, S., Michel, R., Textor, M., and Spencer, N. (2002) Self-assembled monolayers of dodecyl and hydroxy-dodecyl phosphates on both smooth and rough titanium and titanium oxide surfaces. *Langmuir 18*, 3537−3548.
(25) Raman, A., Dubey, M., Gouzman, I., and Gawalt, E. S. (2006) Formation of self-assembled monolayers of alkylphosphonic acid on the native oxide surface of SS316L. *Langmuir 22*, 6469−6472.
(26) Raman, A., and Gawalt, E. S. (2007) Self-assembled monolayers of alkanoic acids on the native oxide surface of SS316L by solution deposition. *Langmuir 23*, 2284−2288.
(27) Adden, N., Gamble, L. J., Castner, D. G., Hoffmann, A., Gross, G., and Menzel, H. (2006) Phosphonic acid monolayers for binding of bioactive molecules to titanium surfaces. *Langmuir 22*, 8197−8204.
(28) Zorn, G., Gotman, I., Gutmanas, E., Adadi, R., Salitra, G., and Sukenik, C. (2005) Surface modification of Ti45Nb alloy with an alkylphosphonic acid self-assembled monolayer. *Chem. Mater. 17*, 4218−4226.
(29) Boissezon, R., Muller, J., Beaugeard, V., Monge, S., and Robin, J.-J. (2014) Organophosphonates as anchoring agents onto metal oxide-based materials: Synthesis and applications. *RSC Adv. 4*, 35690−35707.
(30) Gnauck, M., Jaehne, E., Blaettler, T., Tosatti, S., Textor, M., and Adler, H.-J. P. (2007) Carboxy-terminated oligo(ethylene glycol)−alkane phosphate: Synthesis and self-assembly on titanium oxide surfaces. *Langmuir 23*, 377−381.
(31) Foster, T. T., Alexander, M. R., Leggett, G. J., and McAlpine, E. (2006) Friction force microscopy of alkylphosphonic acid and carboxylic acids adsorbed on the native oxide of aluminum. *Langmuir 22*, 9254−9259.
(32) Gawalt, E. S., Avaltroni, M. J., Koch, N., and Schwartz, J. (2001) Self-assembly and bonding of alkanephosphonic acids on the native oxide surface of titanium. *Langmuir 17*, 5736−5738.
(33) Hanson, E. L., Schwartz, J., Nickel, B., Koch, N., and Danisman, M. F. (2003) Bonding self-assembled, compact organophosphonate monolayers to the native oxide surface of silicon. *J. Am. Chem. Soc. 125*, 16074−16080.
(34) Kingshott, P., Wei, J., Bagge-Ravn, D., Gadegaard, N., and Gram, L. (2003) Covalent attachment of poly(ethylene glycol) to surfaces, critical for reducing bacterial adhesion. *Langmuir 19*, 6912−6921.
(35) Bremmell, K. E., Kingshott, P., Ademovic, Z., Winther-Jensen, B., and Griesser, H. J. (2006) Colloid probe AFM investigation of interactions between fibrinogen and PEG-like plasma polymer surfaces. *Langmuir 22*, 313−318.
(36) Malisova, B., Tosatti, S., Textor, M., Gademann, K., and Zürcher, S. (2010) Poly(ethylene glycol) adlayers immobilized to metal oxide substrates through catechol derivatives: Influence of assembly conditions on formation and stability. *Langmuir 26*, 4018−4026.
(37) Gölander, C. G., Herron, J., Lim, K., Claesson, P., Stenius, P., and Andrade, J. D. (1992) Properties of immobilized PEG films and the interaction with proteins. In *Poly(ethylene glycol) Chemistry* (Harris, J. M., Ed.) pp 221−245, Springer, New York.
(38) Emoto, K., Harris, J. M., and Van Alstine, J. M. (1996) Grafting poly(ethylene glycol) epoxide to amino-derivatized quartz: effect of temperature and pH on grafting density. *Anal. Chem. 68*, 3751−3757.
(39) Malmsten, M., Emoto, K., and Van Alstine, J. M. (1998) Effect of chain density on inhibition of protein adsorption by poly(ethylene glycol) based coatings. *J. Colloid Interface Sci. 202*, 507−517.
(40) Sofia, S. J., Premnath, V., and Merrill, E. W. (1998) Poly(ethylene oxide) grafted to silicon surfaces: grafting density and protein adsorption. *Macromolecules 31*, 5059−5070.
(41) Pasche, S., De Paul, S. M., Vörös, J., Spencer, N. D., and Textor, M. (2003) Poly(L-lysine)-graft-poly(ethylene glycol) assembled

DOI: 10.1021/acs.bioconjchem.5b00208
Bioconjugate Chem. 2015, 26, 1359−1369

monolayers on niobium oxide surfaces: a quantitative study of the influence of polymer interfacial architecture on resistance to protein adsorption by TOF-SIMS and in situ OWLS. *Langmuir 19*, 9216−9225.
(42) Billinger, M., Buddeberg, F., Hubbell, J. A., Elbert, D. L., Schaffner, T., Mettler, D., Windecker, S., Meier, B., and Hess, O. M. (2006) Polymer stent coating for prevention of neointimal hyperplasia. *J. Invasive Cardiol. 18*, 423−426.
(43) Huang, N.-P., Michel, R., Voros, J., Textor, M., Hofer, R., Rossi, A., Elbert, D. L., Hubbell, J. A., and Spencer, N. D. (2001) Poly(L-lysine)-g-poly(ethylene glycol) layers on metal oxide surfaces: surface-analytical characterization and resistance to serum and fibrinogen adsorption. *Langmuir 17*, 489−498.
(44) Emoto, K., Van Alstine, J. M., and Harris, J. M. (1998) Stability of poly(ethylene glycol) graft coatings. *Langmuir 14*, 2722−2729.
(45) Thissen, P., Valtiner, M., and Grundmeier, G. (2009) Stability of phosphonic acid self-assembled monolayers on amorphous and single-crystalline aluminum oxide surfaces in aqueous solution. *Langmuir 26*, 156−164.
(46) Mani, G., Johnson, D. M., Marton, D., Dougherty, V. L., Feldman, M. D., Patel, D., Ayon, A. A., and Agrawal, C. M. (2008) Stability of self-assembled monolayers on titanium and gold. *Langmuir 24*, 6774−6784.
(47) Kaufmann, C. R., Mani, G., Marton, D., Johnson, D. M., and Agrawal, C. M. (2010) Long-term stability of self-assembled monolayers on 316L stainless steel. *Biomed. Mater. 5*, 025008.
(48) Zoulalian, V., Zürcher, S., Tosatti, S., Textor, M., Monge, S., and Robin, J.-J. (2009) Self-assembly of poly(ethylene glycol)−poly(alkyl phosphonate) terpolymers on titanium oxide surfaces: synthesis, interface characterization, investigation of nonfouling properties, and long-term stability. *Langmuir 26*, 74−82.
(49) Stoebner, S. E., and Mani, G. (2012) Effect of processing methods on drug release profiles of anti-restenotic self-assembled monolayers. *Appl. Surf. Sci. 258*, 5061−5072.
(50) Chan, J. W., Petersen, L. K., Lewis, D. R., Moghe, P. V., and Uhrich, K. E. Amphiphilic nanoassemblies as restenosis therapeutics to suppress smooth muscle cell proliferation. Unpublished results.
(51) Wang, J., Plourde, N. M., Iverson, N., Moghe, P. V., and Uhrich, K. E. (2007) Nanoscale amphiphilic macromolecules as lipoprotein inhibitors: the role of charge and architecture. *Int. J. Nanomed. 2*, 697−705.
(52) Hehir, S., Plourde, N. M., Gu, L., Poree, D. E., Welsh, W. J., Moghe, P. V., and Uhrich, K. E. (2012) Carbohydrate composition of amphiphilic macromolecules influences physicochemical properties and binding to atherogenic scavenger receptor A. *Acta Biomater. 8*, 3956−3962.
(53) Chnari, E., Lari, H. B., Tian, L., Uhrich, K. E., and Moghe, P. V. (2005) Nanoscale anionic macromolecules for selective retention of low-density lipoproteins. *Biomaterials 26*, 3749−3758.
(54) Chnari, E., Nikitczuk, J. S., Uhrich, K. E., and Moghe, P. V. (2006) Nanoscale anionic macromolecules can inhibit cellular uptake of differentially oxidized LDL. *Biomacromolecules 7*, 597−603.
(55) Djordjevic, J., Barch, M., and Uhrich, K. E. (2005) Polymeric micelles based on amphiphilic scorpion-like macromolecules: novel carriers for water-insoluble drugs. *Pharm. Res. 22*, 24−32.
(56) Gu, L., Faig, A., Abdelhamid, D., and Uhrich, K. (2014) Sugar-based amphiphilic polymers for biomedical applications: from nanocarriers to therapeutics. *Acc. Chem. Res. 47*, 2867−2877.
(57) Iverson, N. M., Sparks, S. M., Demirdirek, B., Uhrich, K. E., and Moghe, P. V. (2010) Controllable inhibition of cellular uptake of oxidized low-density lipoprotein: structure−function relationships for nanoscale amphiphilic polymers. *Acta Biomater. 6*, 3081−3091.
(58) Lewis, D. R., Kholodovych, V., Tomasini, M. D., Abdelhamid, D., Petersen, L. K., Welsh, W. J., Uhrich, K. E., and Moghe, P. V. (2013) In silico design of anti-atherogenic biomaterials. *Biomaterials 34*, 7950−7959.
(59) Lewis, D. R., Petersen, L. K., York, A. W., Zablocki, K. R., Joseph, L. B., Kholodovych, V., Prud'homme, R. K., Uhrich, K. E., and Moghe, P. V. (2015) Sugar-based amphiphilic nanoparticles arrest atherosclerosis in vivo. *Proc. Natl. Acad. Sci. U. S. A. 112*, 2693−2698.
(60) Tian, L., Yam, L., Zhou, N., Tat, H., and Uhrich, K. E. (2003) Amphiphilic scorpion-like macromolecules: design, synthesis, and characterization. *Macromolecules 37*, 538−543.
(61) Sparks, S. M. (2011) Design, synthesis, and utility of fuctionalized nanoscale amphiphilic macromolecules for biomedical applications. Thesis. Rutgers University, Piscataway, NJ.
(62) Damodaran, V. B., Fee, C. J., Ruckh, T., and Popat, K. C. (2010) Conformational studies of covalently grafted poly(ethylene glycol) on modified solid matrices using X-ray photoelectron spectroscopy. *Langmuir 26*, 7299−7306.
(63) Zhu, B., Eurell, T., Gunawan, R., and Leckband, D. (2001) Chain-length dependence of the protein and cell resistance of oligo(ethylene glycol)-terminated self-assembled monolayers on gold. *J. Biomed. Mater. Res. 56*, 406−416.
(64) Saxer, S., Portmann, C., Tosatti, S., Gademann, K., Zürcher, S., and Textor, M. (2010) Surface assembly of catechol-functionalized poly(L-lysine)-graft-poly(ethylene glycol) copolymer on titanium exploiting combined electrostatically driven self-organization and biomimetic strong adhesion. *Macromolecules 43*, 1050−1060.
(65) Choudhary, S., Haberstroh, K. M., and Webster, T. J. (2007) Enhanced functions of vascular cells on nanostructured Ti for improved stent applications. *Tissue Eng. 13*, 1421−1430.
(66) Eral, H., and Oh, J. (2013) Contact angle hysteresis: A review of fundamentals and applications. *Colloid Polym. Sci. 291*, 247−260.
(67) Williams, R. (2011) *Surface Modification of Biomaterials: Methods Analysis and Applications*, 1st ed., Woodhead Publishing, Cambridge, UK.
(68) Schwartz, D. K. (2001) Mechanisms and kinetics of self-assembled monolayer formation. *Annu. Rev. Phys. Chem. 52*, 107−137.
(69) Kaewsaiha, P., Matsumoto, K., and Matsuoka, H. (2004) Synthesis and nanostructure of strong polyelectrolyte brushes in amphiphilic diblock copolymer monolayers on a water surface. *Langmuir 20*, 6754−6761.
(70) Mouri, E., Furuya, Y., Matsumoto, K., and Matsuoka, H. (2004) Hydrophilic chain length dependence of the ionic amphiphilic polymer monolayer structure at the air/water interface. *Langmuir 20*, 8062−8067.
(71) Kingshott, P., Thissen, H., and Griesser, H. J. (2002) Effects of cloud-point grafting, chain length, and density of PEG layers on competitive adsorption of ocular proteins. *Biomaterials 23*, 2043−2056.
(72) Hähner, G., Hofer, R., and Klingenfuss, I. (2001) Order and orientation in self-assembled long chain alkanephosphate monolayers adsorbed on metal oxide surfaces. *Langmuir 17*, 7047−7052.
(73) Hofer, R., Textor, M., and Spencer, N. (2001) Alkyl phosphate monolayers, self-assembled from aqueous solution onto metal oxide surfaces. *Langmuir 17*, 4014−4020.
(74) Motornov, M., Sheparovych, R., Tokarev, I., Roiter, Y., and Minko, S. (2007) Nonwettable thin films from hybrid polymer brushes can be hydrophilic. *Langmuir 23*, 13−19.
(75) Israelachvili, J., and Tabor, D. (1972) The measurement of van der Waals dispersion forces in the range 1.5 to 130 nm. *Proc. R. Soc. A 331*, 19−38.
(76) Tosatti, S. G. P. (2003) Functionalized titanium surfaces for biomedical applications: Physico-chemical characterization and biological in vitro evaluation. Thesis. ETH Zürich.
(77) Yang, G., Amro, N. A., Starkewolfe, Z. B., and Liu, G.-Y. (2004) Molecular-level approach to inhibit degradations of alkanethiol self-assembled monolayers in aqueous media. *Langmuir 20*, 3995−4003.
(78) Chatterjee, S. (1992) Role of oxidized human plasma low density lipoproteins in atherosclerosis: effects on smooth muscle cell proliferation. *Mol. Cell. Biochem. 111*, 143−147.
(79) Rutherford, R. B., and Ross, R. (1976) Platelet factors stimulate fibroblasts and smooth muscle cells quiescent in plasma serum to proliferate. *J. Cell Biol. 69*, 196−203.
(80) Lewis, D. R., Petersen, L. K., York, A. W., Ahuja, S., Uhrich, K. E., Haser, P. B., and Moghe, P. V. Nanotherapeutics for inhibition of

DOI: 10.1021/acs.bioconjchem.5b00208
Bioconjugate Chem. 2015, 26, 1359−1369

atherogenesis and modulation of inflammation in atherosclerotic plaques.
(81) Petersen, L. K., York, A. W., Zablocki, K. R., Fan, C., Lewis, D. R., Uhrich, K. E., Prud'homme, R. K., Haser, P. B., Graham, A. M., and Moghe, P. V. (2013) AIChE Annual Meeting, San Francisco, CA.
(82) Casscells, W. (1992) Migration of smooth muscle and endothelial cells. Critical events in restenosis. *Circulation 86*, 723−729.
(83) Palik, E. D. (1998) *Handbook of Optical Constants of Solids*, Vol. 3, Academic Press, New York.
(84) Kharlampieva, E., Kozlovskaya, V., Chan, J., Ankner, J. F., and Tsukruk, V. V. (2009) Spin-assisted layer-by-layer assembly: variation of stratification as studied with neutron reflectivity. *Langmuir 25*, 14017−14024.

DOI: 10.1021/acs.bioconjchem.5b00208
Bioconjugate Chem. 2015, 26, 1359−1369